Chemical Physics Letters 463 (2008) 112–116

Contents lists available at ScienceDirect

Chemical Physics Letters

journal homepage: www.elsevier.com/locate/cplett

QM–MM investigation of the reaction products between nitroxyl and O_2 in aqueous solution

Carlos M.A. Guardia, Mariano C. González Lebrero, Sara E. Bari, Darío A. Estrin *

Departamento de Química Inorgánica, Analítica y Química Física/INQUIMAE, Facultad de Ciencias Exactas y Naturales, Universidad de Buenos Aires/CONICET, Ciudad Universitaria, Pab. II, P. 1, C1428EHA Buenos Aires, Argentina

ARTICLE INFO

Article history:
Received 15 July 2008
In final form 18 August 2008
Available online 22 August 2008

ABSTRACT

By means of combined quantum-classical molecular (QM/MM) dynamics simulations, we investigated the structural properties and the vibrational spectra in aqueous solution of four possible intermediate species of the oxidation of nitroxyl (HNO/NO^-) by dioxygen, the *cis*- and *trans*-isomers of peroxynitrous acid and nitroxyl-dioxygen adduct. Our study suggests that Raman spectroscopy will provide signals for discrimination between the peroxynitrous acid isomers from both adducts, and that infrared spectroscopy will probably assist the discrimination between the *cis*-peroxynitrous acid isomer from the other compounds considered. This application of hybrid simulation methods highlights the benefits of explicit solvent representations.

1. Introduction

Among the reactive nitrogen oxide species (RNOs), nitroxyl has emerged as a particularly relevant specie in the last decade, due to the participation of nitroxyl donors in relevant biochemical processes as the enhancement of the myocardial contractility [1], vasodilation [2–4], the inhibition of platelet aggregation [5], the inhibition of lipid peroxidation both in yeast and *in vitro* model systems [6], and citotoxicity [7,8]. The use of nitroxyl donors allows overcoming the limitations imposed by the instability of the isolated molecule [9]. This prompted interest in the investigation of new potential donors, with specifically tuned properties. The most extensively used nitroxyl donor, which opened roads for nitroxyl chemistry and is currently considered as the best candidate for pharmacologic purposes, is Angeli's salt ($Na_2N_2O_3$, AS) [10–12]. The generation of HNO from the AS (R1) and from other different sources has been the subject of many studies, both from theoretical (electronic structure calculations and continuum solvent models) [13,14] and experimental perspectives [11,15,16].

$$Na_2N_2O_3 + H^+ \rightarrow [NaHN_2O_3] \rightarrow HNO + NaNO_2 \quad (k_{obs} = 4.6 \times 10^{-4}\ s^{-1} \text{ at pH } 4\text{–}8) \qquad (R1)$$

A fast reaction of dimerization followed by dehydration is one of the main sinks of nitroxyl (R2)

$$2HNO \rightarrow H_2N_2O_2 \rightarrow N_2O + H_2O \quad (k_{obs} = 8 \times 10^6\ M^{-1}\ s^{-1}) \qquad (R2)$$

Because of the magnitude of the rate of the dimerization process [17], it is clear that it should compete with other reactions under most experimental conditions. The hydrogen bonding and IR spectra of HNO dimer have been recently studied by electronic structure calculations [18].

Another fascinating and unique aspect of HNO chemistry involves the peculiar features of its acid–base equilibrium. Unlike NO, the ground electronic state of nitroxyl is a singlet (^1HNO), and its conjugate base, NO^-, isoelectronic with oxygen, presents a triplet ground state ($^3NO^-$). This aspect constituted an unnoticed difficulty in the pioneering determinations of pK_a, yielding fluctuating values over decades, to finally reach consensus on $pK_a = 11.4$ by two independent techniques [17,19]. In the same context of complexity HNO basic chemistry, some theoretical calculations were performed to achieve reduction potentials for some reactions where HNO is actually implicated [20]. At concentrations higher than 30 μM of AS the fast dimerization process (R2) controls product formation, and the concentration of the conjugate base is negligible, whereas below 5 μM of AS more than 99% of HNO will be consumed by O_2 [21].

One of the most important and relevant biological aspects in HNO chemistry is associated to its electrophilic character. These reactions are usually very selective, being thiols and proteins with thiol groups [22], olefinic species [23] and metalloproteins [24] the major biologically relevant targets of nitroxyl. The interactions of HNO with CO and NO have also been computationally studied [25,26].

On the other hand, HNO may also react with dioxygen. One previous report indicates that HNO reacts with O_2, since a decomposing solution of AS was found to consume O_2 [27]. The reaction of nitroxyl species with dioxygen is expected to be highly dependent

* Corresponding author. Fax: +54 11 45763341.
E-mail address: dario@qi.fcen.uba.ar (D.A. Estrin).

0009-2614/$ - see front matter © 2008 Elsevier B.V. All rights reserved.
doi:10.1016/j.cplett.2008.08.064

on its spin state. The ground state of the nitroxyl anion, $^3NO^-$, is known to react with O_2 to produce peroxynitrite, $ONOO^-$ [12,17], in a diffusion controlled process (R3) isoelectronic with the well-known and characterized reaction of nitric oxide with superoxide O_2^- (R4) [28,29]

$$^3NO^- + {}^3O_2 \rightarrow ONOO^- \quad (k_{obs} = 2.7 \times 10^9\ M^{-1}\ s^{-1}) \tag{R3}$$

$$NO + O_2^- \rightarrow ONOO^- \quad (k_{obs} = 4\text{–}7 \times 10^9\ M^{-1}\ s^{-1}) \tag{R4}$$

The biological relevance of these reactions is highly dependent on the physiological concentration of reactants. Due to the high pK_a value of HNO, $^3NO^-$ concentrations are negligible under physiological conditions, and radical oxygen species (ROS) detoxification systems (if their functionality is not altered) avoid the increase in O_2^- concentration. So, the direct oxidation of HNO with O_2 seems to be a more feasible process for peroxynitrite formation. Experimental studies [30–32], suggested that the equimolar reaction between AS and molecular oxygen yields a potent two-electron oxidant, with a reaction profile different from that of peroxynitrite. Miranda and coworkers suggested the formation of new, uncharacterized, peroxynitrous acid isomers and HNO/O_2 adducts as putative reaction products, on the basis of chemical reactivity. These species are expected to be stable intermediates, according to experimental and computational evidence [32–34].

In this work, we employed state-of-the-art hybrid quantum-classical (QM–MM) computer simulation tools to obtain microscopic information of this relevant reaction. More specifically, the aim of this work is to provide spectroscopy predictions of four possible intermediate species, namely the *cis*- and *trans*-isomers of peroxynitrous acid and the *cis*- and *trans*-isomers of the HNO/O_2 adduct (Fig. 1) in aqueous solution.

2. Model and simulation methods

Our computational scheme was constructed by partitioning the system into quantum-mechanical (QM) and classical-mechanical (MM) subsystems. Considering a configuration of N_c atoms in the MM subsystem with coordinates and partial charges $\{R_l,\ q_l,\ l = 1,\ldots,N_c\}$ and N_q atoms in the QM sub-system with coordinates and nuclear charges $\{\tau_\alpha,\ z_\alpha,\ \alpha = 1,\ldots,N_q\}$, we proposed the expression Eq. (1) for the ground state, Born–Oppenheimer potential energy surface that drives the dynamics of the nuclei

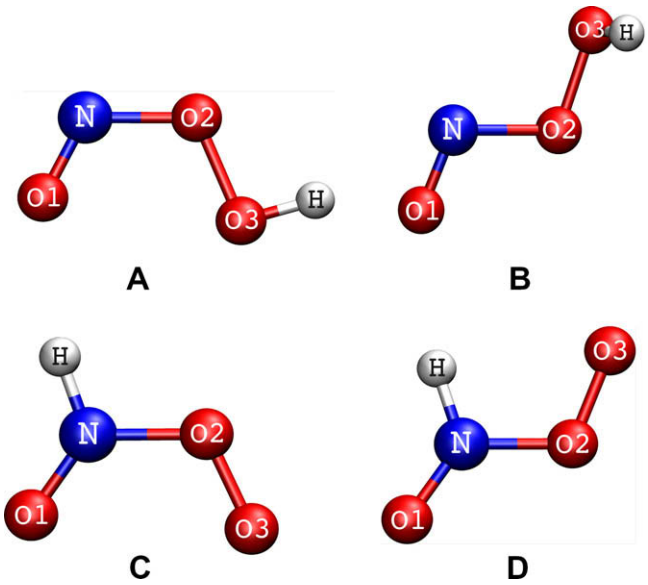

Fig. 1. Structures proposed for the reaction product of HNO with O_2.

$$E[\{R_i\},\{\tau_\alpha\}] = E_{KS} + E_{QM-MM} + E_{MM} \tag{1}$$

where the first term is a purely QM piece given by the standard Kohn–Sham expression [35]. The second term in Eq. (1) accounts for the coupling of the QM and MM subsystems and is given by

$$E_{QM-MM} = \sum_{l=1}^{N_c} q_l \int \frac{\rho(r)}{|r - R_l|}\mathrm{d}r + \sum_{l=1}^{N_c} \times \sum_{\alpha=1}^{N_q} \left[\upsilon_{LJ}(|R_l - \tau_\alpha|) + \frac{q_l z_\alpha}{|R_l - \tau_\alpha|} \right] \tag{2}$$

where υ_{LJ} is the Lennard–Jones potential between the classical and quantum part of the system and $\rho(r)$ is the electron density of the QM subsystem. The last term in Eq. (1) represents the potential energy contribution from the classical solvent potential, treated with the TIP4P mean-field [36]. For the QM region, computations were performed at the generalized gradient approximation (GGA) level, using the PBE combination of exchange and correlation functionals [37]. Gaussian basis sets of double-ζ plus polarization quality were employed for the expansion of the one-electron orbitals [36]. The electronic density was also expanded in an auxiliary basis set [38]; the coefficients for the fit were computed by minimizing the error in the Coulomb repulsion energy. The use of this procedure results in an important speedup of the computations. The electronic density was computed every MD step.

2.1. Molecular dynamics Simulations

In all our simulation experiments, the coordinate Verlet algorithm [39] was employed to integrate Newton's equations of motion with a time step of 0.1 fs for simulations. Constraints associated with the intramolecular distances in water were treated using the Shake algorithm [40]. The Lennard–Jones parameters for the quantum subsystem atoms are ε and σ of 0.200 and 0.155 kcal/mol, and 3.900 and 3.154 Å, for N and O, respectively. The solute was solvated in a cubic box of size $a = 24$ Å, containing 497 water molecules. Periodic boundary conditions with a group cutoff were used for solvent–solvent and solvent–solute interactions [41]. Initial configurations were generated from preliminary 100 ps classical equilibration runs in which the quantum solute was replaced by a rigid species with partial charges obtained from a Mulliken population analysis. At $t = 0$, the classical solute is replaced by one of the four compounds each time described at the DFT level, according to the hybrid methodology described above. An additional 1 ps of equilibration was performed using the QM–MM scheme. During the simulations, the temperature was held constant at 300 K by the Berendsen thermostat [42]. The solute and the rest of the system were coupled separately to the temperature bath. In all cases, 10 ps of dynamics were used for production runs.

2.2. IR Spectra Simulation

The IR spectrum of a system can be predicted using different computational techniques. The usual method is to obtain the normal-mode frequencies and intensities from the diagonalization of the Hessian matrix. This method is useful for molecules in the gas phase. The inclusion of solvent effects can be achieved with continuum solvent models [43]. However, this scheme may present flaws in cases in which there are strong specific solute–solvent interactions. The IR spectrum can also be computed directly from a molecular dynamics simulation using explicit solvent molecules. The infrared absorption $I(\omega)$ is related to the Fourier transform of the dipole autocorrelation function $C(t)$ [44,45] by

$$I(\omega) = \frac{1}{2\pi}\int_{-\infty}^{+\infty} C(t)\mathrm{e}^{-\mathrm{i}\omega t}\mathrm{d}t \tag{3}$$

The correlation function of a stationary property is independent of the time origin. This type of function depends on the interval between the correlated time values. In the discrete case, the dipole moment autocorrelation function $C(\tau)$ is then expressed by

$$C(\tau) = \frac{1}{T-\tau} \sum_{t_0=0}^{T-\tau-1} \mu(t_0) \cdot \mu(t_0+\tau) \quad (4)$$

where μ is the dipole moment at time t, T is the total number of time steps in the simulation, τ is the time interval, and t_0 is the time origin. In some cases, in order to facilitate spectral assignments and to obtain the vibrational frequencies corresponding to each normal mode in the isolated species, it is convenient to transform the dynamical trajectory into the normal modes coordinates of the isolated solute [41].

This computational QM–MM scheme [46] has been applied previously [41,47] and it is expected to take into account both solvent and anharmonicity effects. This requisite is almost indispensable if our goal is to distinguish between four structural isomers of this unknown reactive nitrogen oxide species in solution.

To investigate solvent effects on the vibrational properties of the four postulated compounds shown in the Fig. 1, we performed QM–MM molecular dynamics simulations at the PBE–DFT level, with the mean-field TIP4P potential for modelling the solvent. In addition, we have also performed additional simulations of the isolated molecules and of the solvated species using the implicit polarizable dielectric solvent model (PCM) at the PBE level, as implemented in Gaussian 98 [48], to establish the effects of explicit solvent incorporation to these particular systems.

3. Results and discussion

Calculated vibrational properties of the isolated molecules and of the solvated species, using the implicit polarizable dielectric solvent model and the molecular dynamics approach, are presented in Table 1. As a preliminary result, no *cis–trans* conformational transitions were observed in the MD simulations.

In the first place, it should be noted that not all the calculated frequencies can be assigned to simple bending or stretching vibrational modes, since these molecules have a low level of symmetry and their constitutive atoms are similar, resulting in several vibrational modes which may involve several atoms. Secondly, the analysis of the MD frequencies of each compound was restricted to the highest frequency values, not only for the reason above, but also because of the presence of solvent and/or matrix component bands in the low wavenumber region.

The harmonic vibrational frequencies obtained from the isolated compounds and from the implicit solvent description are,

Table 1
Vibrational frequencies (cm^{-1}), IR intensities and Raman activities (in relative units) for the proponed structures[a]

Type of cal.	Vacuum			PCM			MD	
Data	Freq	IR	Raman	Freq	IR	Raman	Freq	IR
Compound A								
ν_1	134	0.601	0.048	120	0.341	0.03	–	–
ν_2	237	0.049	0.064	262	0.017	0.063	–	–
ν_3	396	0.290	0.045	452	6.2e–5	0.002	–	–
ν_4 (NO_2 str)	435	1.7e–5	0.002	479	0.198	0.042	–	–
ν_5	764	0.437	0.121	763	0.283	0.114	754	0.55
ν_6 (O_2O_3 str)	861	0.011	0.055	874	0.006	0.045	919	0.07
ν_7 (HO_2O_3 bend)	1296	0.252	0.048	1287	0.190	0.045	1438	0.21
ν_8 (NO_1 str)	1662	1.000	0.133	1600	0.683	0.179	1654	1.00
ν_9 (O_3H str)	3669	0.449	1.000	3071	1.000	1.000	3358	0.31
Compound B								
ν_1	199	0.073	0.017	190	0.064	0.015	–	–
ν_2	277	0.391	0.064	293	0.385	0.051	–	–
ν_3	314	0.031	0.021	327	0.103	0.038	–	–
ν_4 (NO_2 str)	401	0.210	0.195	386	0.231	0.235	–	–
ν_5	770	0.238	0.049	759	0.281	0.058	771	0.45
ν_6 (O_2O_3 str)	966	0.357	0.042	960	0.361	0.038	963	0.36
ν_7 (HO_2O_3 bend)	1343	0.205	0.075	1316	0.232	0.067	1455	0.12
ν_8 (NO_1 str)	1745	1.000	0.181	1706	1.000	0.321	1708	1.00
ν_9 (O_3H str)	3646	0.179	1.000	3112	0.823	1.000	3364	0.15
Compound C								
ν_1	271	0.022	0.030	308	0.010	0.066	–	–
ν_2	380	0.257	0.007	476	0.067	0.002	–	–
ν_3	481	0.164	0.005	564	0.164	0.004	–	–
ν_4 (NO_2 str)	605	0.077	0.058	725	0.043	0.158	–	–
ν_5	852	0.138	0.030	835	0.261	0.077	832	0.34
ν_6 (O_2O_3 str)	1125	0.666	0.020	1053	0.390	0.029	1050	0.60
ν_7 (O_1NH bend)	1336	0.058	0.043	1309	0.086	0.066	1348	0.27
ν_8 (NO_1 str)	1585	1.000	0.017	1564	0.631	0.049	1585	1.00
ν_9 (NH str)	3295	0.123	1.000	2740	1.000	1.000	3059	0.39
Compound D								
ν_1	222	0.044	0.004	242	0.064	0.006	–	–
ν_2	363	0.093	0.002	361	0.110	0.013	–	–
ν_3	496	0.002	0.162	545	0.003	0.358	–	–
ν_4 (NO_2 str)	701	0.245	0.040	716	0.176	0.024	–	–
ν_5	874	0.053	0.047	876	0.098	0.073	852	0.31
ν_6 (O_2O_3 str)	1108	0.424	0.111	1061	0.618	0.198	1076	0.74
ν_7 (O1NH bend)	1294	0.306	0.021	1273	0.309	0.066	1348	0.28
ν_8 (NO_1 str)	1586	1.000	0.123	1564	1.000	0.413	1563	1.00
ν_9 (NH str)	3102	0.041	1.000	2596	0.434	1.000	2980	0.09

[a] All the calculations have been performed using the DZP basis set, at the PBE–DFT level.

in several cases, very different from the frequencies obtained with our MD/QM–MM scheme, highlighting the role of specific solvent effects in certain vibrational modes of the species considered (eg.: ν_7 in compounds A and B, assigned to HO_2O_3 bending).

The infrared spectra for each compound in aqueous solution, obtained from the PBE–TIP4P simulation are shown in Fig. 2. Each curve corresponds to the Fourier transform of the dipolar moment autocorrelation function.

The NO_1 stretching frequency in the spectra of all species provides a very narrow and intense peak that aids to the discrimination of the four models considering the relative intensity I of the bands νNO_1 and νO_2O_3: while the ratio $I\nu NO_1/I\nu O_2O_3$ is similar among the B, C and D isomers, a quite distinctive ratio is evidenced for model A.

Other particularly interesting case is the relatively low calculated intensity for the X–H (X = O, N) stretching band, the highest frequency computed in each spectrum (ca. 3000 cm^{-1}). The QM–MM computed infrared intensity of this band is very small. Unfortunately, it is not feasible to compute Raman activities from the QM–MM calculations, due to the high computational cost. However, the Raman activity estimated with the continuum calculations with the same functional and basis set used in the previous simulations was exceptionally high (Table 1), in comparison with other bands of the same molecule. This suggests that Raman spectroscopy may be useful to discriminate the isomers A/B from the C/D, which exhibit stretching frequencies in the 3300 and 3000 cm^{-1} range, respectively.

A further insight in the vibrational description of these bonds was used to provide information beyond its low intensity in the calculated IR band. The vibrational density of states of the highest frequency bands is depicted in Fig. 3. Each curve corresponds to the Fourier transform of the velocity for the bond O–H or N–H, according to the case. It is possible to observe, as expected, similar values of frequency and line width.

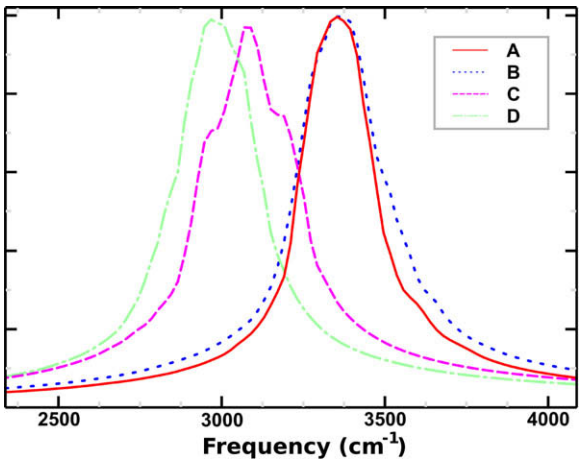

Fig. 3. Vibrational density of states for the highest frequency.

Indeed, the computed properties of the X–H band (X = O, N) strongly reflect structural differences. A summary of selected parameters for this bond, for A and C species is shown in Table 2. Similar effects were observed in the other two compounds, B and D. We observe that the incorporation of the solvent, implicit with PCM or explicit with our QM/MM scheme, causes very remarkable effects in all the parameters involved in the vibration of that bond, namely the distance X–H, the Mulliken charges on the participating atoms, and the vibrational frequency.

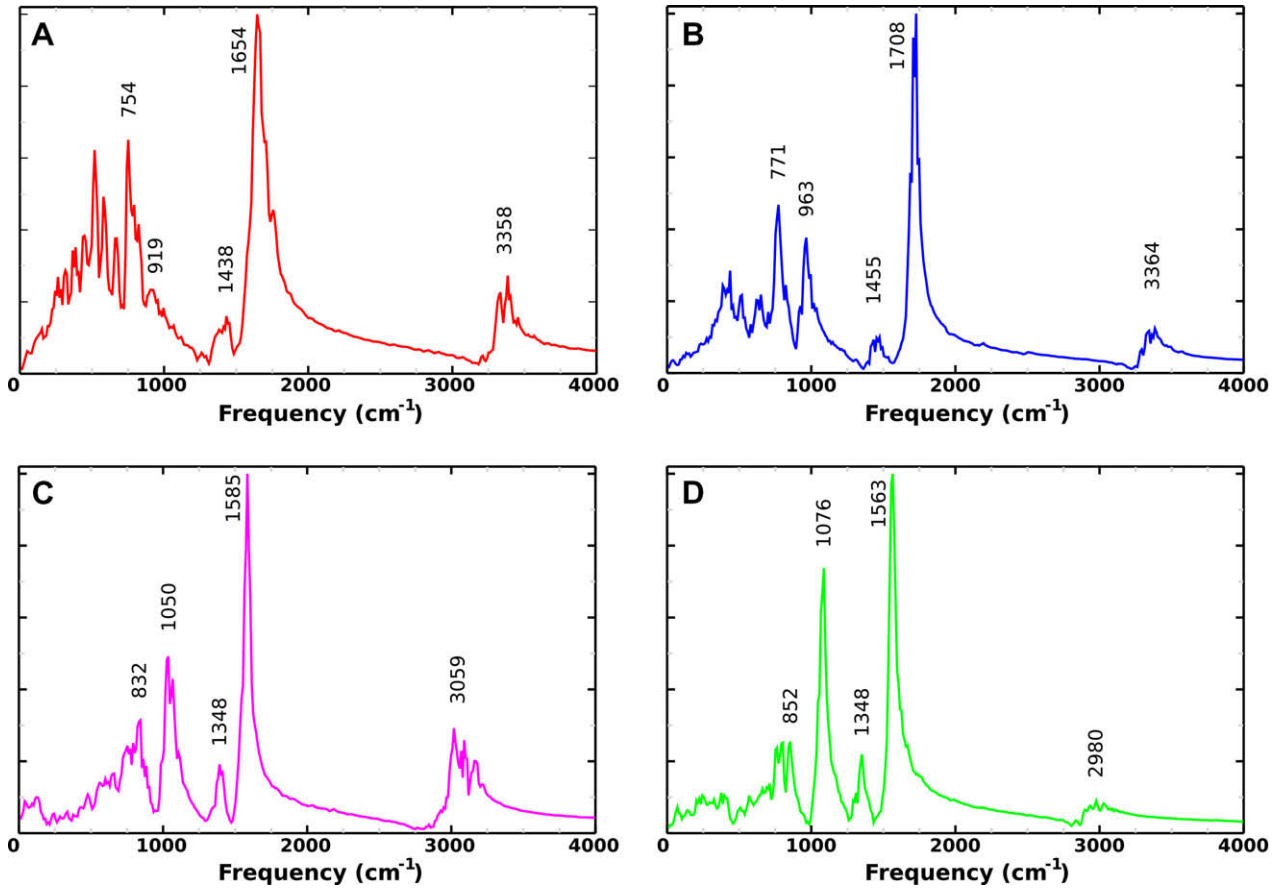

Fig. 2. QM/MM infrared spectra.

Table 2
Structural, vibrational and Mulliken population information for selected X–H {X = O, N} bond in A and C species

	A				C		
	Isolated	PCM	MD–QM/MM[a]		Isolated	PCM	MD–QM/MM[a]
d_{O_3-H} (Å)	0.983	1.011	1.000	d_{N-H} (Å)	1.037	1.071	1.057
q_{O_3-H} (e)	−0.288	−0.321	−0.417	q_N (e)	0.184	0.236	0.063
q_H (e)	0.335	0.406	0.469	q_H (e)	0.283	0.394	0.464
ν_{O_3-H} (cm^{-1})	3669	3071	3358	ν_{N-H} (cm^{-1})	3295	2740	3059

[a] Corresponds to average values along all the simulation time. The frequencies have been obtained as the maxima in the IR spectrum from Fig. 3.

The observed shifts, associated to the incorporation of the solvent in the vibrational frequency, are much larger in the PCM compared to the MD–QM–MM calculations. This is probably due to the poor estimation of specific interactions in the continuum model case. In this particular case, the solvent effect description is essential because solvation has direct implications on the position and intensity of at least one frequency, resulting in distinctive features for these set of calculated spectra. We have demonstrated previously [41], that this particular computational scheme achieved an unmatched spectroscopy and solvation description of peroxynitrite in aqueous solution which allowed to obtain values of vibration frequencies with margins of error not exceeding 4%, with respect to experimental data, while a representation with harmonic and implicit solvent models reached 12% differences with the same input. These results represent a good precedent to the scheme used, and allow us to ensure that the error of the values of the frequencies estimated will be smaller than the separation between homologous bands, allowing to aidding the unequivocal characterization of these compounds.

A thorough and final analysis of our QM–MM results highlights particular bands or regions of bands that differ significantly between each compound. The highest frequency band can be used as a starting point for the differentiation of the compounds considered. In addition, also in the 1600 cm^{-1} and 500–1000 cm^{-1} region there are differences that could facilitate the unequivocal assignment between the proposed products of the reaction between nitroxyl and dioxygen.

4. Conclusions

In this work we have applied state-of-the-art QM–MM computer simulation tools to obtain microscopic information regarding possible reaction products between HNO and O_2, an experimentally elusive, but ubiquitous, reaction relevant to reactive nitrogen oxide species chemistry.

The vibrational spectra in aqueous solution for a set of four isomeric putative reaction products were calculated and our results predict that Raman spectroscopy, specifically of the higher frequency bands (~3000 cm^{-1}), allow the discrimination of isomers A and B from C and D. A detailed comparison of the rest of the spectra could allow to achieve a complete differentiation. At the same time, this work showed that implicit solvent models do not describe correctly the solvent participation in this case. The solvation phenomenon requires an explicit solvent description, as the included in our QM–MM method.

Acknowledgments

This work was partially supported by the University of Buenos Aires, Agencia Nacional de Promoción Científica y Tecnológica (Project PICT 25667), and CONICET (PIP 5218). DAE acknowledges financial support from a John Simon Guggenheim fellowship.

References

[1] D.A. Wink et al., Am. J. Physiol., Heart Circ. Physiol. 285 (2003) H2264.
[2] A. Ellis, C. Li, M.J. Rand, Br. J. Pharmacol. 129 (2000) 315.
[3] J.C. Wanstall, T.K. Jeffery, A. Gambino, F. Lovren, C.R. Triggle, Br. J. Pharmacol. 134 (2001) 463.
[4] J.M. Fukuto, G.C. Wallace, R. Hszieh, G. Chaudhuri, Biochem. Pharmacol. 43 (1992) 607.
[5] E. Bermejo, D.A. Saenz, F. Alberto, R.E. Rosenstein, S.E. Bari, M.A. Lazzari, Thromb. Haemost. 94 (2005) 578.
[6] B.E. Lopez, M. Shinyashiki, T.H. Han, J.M. Fukuto, Free Radical Biol. Med. 42 (2007) 482.
[7] D.A. Wink et al., Arch. Biochem. Biophys. 351 (1998) 66.
[8] N. Paolocci et al., Pharmacol. Ther. 113 (2007) 442.
[9] K.M. Miranda, H.T. Nagasawa, J.P. Toscano, Curr. Top. Med. Chem. 5 (2005) 649.
[10] A. Angeli, Gazz. Chim. Ital. 33 (1903) 245.
[11] F.T. Bonner, B. Ravid, Inorg. Chem. 14 (1975) 558.
[12] C.E. Donald, M.N. Hughes, J.M. Thompson, F.T. Bonner, Inorg. Chem. 25 (1986) 2676.
[13] A.S. Dutton, J.M. Fukuto, K.N. Houk, J. Am. Chem. Soc. 126 (2004) 3795.
[14] A.S. Dutton, C.P. Suhrada, K.M. Miranda, D.A. Wink, J.M. Fukuto, K.N. Houk, Inorg. Chem. 45 (2006) 2448.
[15] S.I. Liochev, I. Fridovich, Free. Radical Biol. Med. 24 (2003) 1399.
[16] C. Amatore, S. Arbault, C. Ducrocq, S. Hu, I. Tapsoba, Chem. Med. Chem. 2 (2007) 898.
[17] V. Shafirovich, S.V. Lymar, Proc. Natl. Acad. Sci. 99 (2002) 7340.
[18] Y. Liu, W. Liu, H. Li, J. Liu, Y. Yang, J. Phys. Chem. A 110 (2006) 11760.
[19] M.D. Bartberger et al., Proc. Natl. Acad. Sci. 99 (2002) 10958.
[20] A.S. Dutton, J.M. Fukuto, K.N. Houk, Inorg. Chem. 44 (2005) 4024.
[21] K.M. Miranda et al., Proc. Natl. Acad. Sci. 100 (2003) 9196.
[22] M.P. Doyle, S.N. Mahapatro, R.D. Broene, J.K. Guy, J. Am. Chem. Soc. 110 (1988) 593.
[23] H.E. Ensley, S. Mahadevan, Tetrahedron Lett. 30 (1989) 3255.
[24] P.J. Farmer, F. Sulc, J. Inorg. Biochem. 99 (2005) 166.
[25] A.Y. Li, J. Phys. Chem A. 110 (2006) 10805.
[26] G.A. Poskrebyshev, V. Shafirovich, S.V. Lymar, J. Am. Chem. Soc. 126 (2004) 891.
[27] J.M. Fukuto, A.J. Hobbs, L.J. Ignarro, Biochem. Biophys. Res. Commun. 196 (1993) 707.
[28] H. Ischiopoulos, L. Zhu, J. Beckman, Arch. Biochem. Biophys. 298 (1992) 446.
[29] G.L. Squadrito, W.A. Pryor, Free. Radical. Biol. Med. 25 (1998) 392.
[30] K.M. Miranda et al., J. Biol. Chem. 276 (2001) 1720.
[31] K.M. Miranda et al., Arch. Biochem. Biophys. 401 (2002) 134.
[32] K.M. Miranda et al., J. Am. Chem. Soc. 127 (2005) 722.
[33] J.M. Tsai, J.G. Harrison, J.C. Martin, T.P. Hamilton, M. van der Woerd, M.J. Jablonsky, J.S. Beckman, J. Am. Chem. Soc. 116 (1994) 4115.
[34] S. Padmaja, R. Kissner, P.L. Bounds, W.H. Koppenol, Helv. Chim. Acta 81 (1998) 1201.
[35] W. Kohn, L.J. Sham, Phys. Rev. A 140 (1965) 1133.
[36] W.L. Jorgensen, J. Chandrasekhar, J.D. Madura, R. Impey, M.L. Klein, J. Chem. Phys. 79 (1983) 926.
[37] J.P. Perdew, K. Burke, M. Ernzerhof, Phys. Rev. Lett. 77 (1996) 3865.
[38] N. Godbout, D.R. Salahub, J. Andzelm, E. Wimmer, Can. J. Chem. 70 (1992) 560.
[39] M.P. Allen, D.J. Tildesley, Computer Simulation of Liquids, Clarendon, Oxford, 1987.
[40] J.P. Ryckaert, G. Ciccotti, H.J.C. Berendsen, J. Comput. Phys. 23 (1977) 327.
[41] M.C. González Lebrero, L.L. Perissinotti, D.A. Estrin, J. Phys. Chem. A 109 (2005) 9598.
[42] H.J.C. Berendsen, J.P.M. Postma, W.F. van Gunsteren, A. Di Nola, J.R. Haak, J. Chem. Phys. 81 (1984) 3684.
[43] M. Cossi, V. Barone, R. Cammi, J. Tomasi, J. Chem. Phys. Lett. 255 (1996) 327.
[44] A.R. Leach, Molecular Modelling: Principles and Applications, Prentice-Hall, New York, 2001.
[45] D.W. Noid, M.L. Koszykowsi, R.A. Marcus, J. Chem. Phys. 67 (1977) 404.
[46] M.D. Elola, D. Laria, D.A. Estrin, J. Phys. Chem. A 103 (1999) 5105.
[47] D.E. Bikiel, F. di Salvo, M.C. González Lebrero, F. Doctorovich, D.A. Estrin, Inorg. Chem. 44 (2005) 5286.
[48] M.J. Frisch et al., Gaussian 98, Revision A.1, Gaussian, Inc., Pittsburgh, PA, 1998.